Eur. Phys. J. B **23**, 405–411 (2001)

THE EUROPEAN PHYSICAL JOURNAL B

EDP Sciences

Coupling effects of layers on spin transport in $ZnSe/Zn_{1-x}Mn_xSe$ heterostructures

F. Zhai[1,2,a], Y. Guo[1], and B.-L. Gu[1,2]

[1] Department of Physics, Tsinghua University, Beijing 100084, PR China
[2] Center for Advanced Study, Tsinghua University, Beijing 100084, PR China

Received 28 April 2001

Abstract. By use of the scattering matrix method, we investigate the coupling effects of layers on spin-polarized transport through semimagnetic semiconductor heterostructures with triple paramagnetic layers. Due to the coupling between double non-magnetic layers or among triple paramagnetic layers, spin tunneling exhibits interesting and complex features, which are determined by the structural configuration, the external fields as well as the spin orientations. It is shown that for electrons with either spin orientation tunneling through the symmetric or asymmetric heterostructures with triple paramagnetic layers, transmission resonances can approach the optimum under several biases. Moreover, for asymmetric structures, the resonant enhancement can occur under both several positive and negative biases. The spin-dependent resonant enhancement is also clearly reflected in the current density. In addition, for spin electrons traversing the multilayer heterostructure, the resonant splitting occurs in the transmission, which shows rich variations with the bias. These interesting results may be helpful to the development of spintronic devices.

PACS. 73.40.Gk Tunneling – 75.50.Pp Magnetic semiconductors

1 Introduction

As an alternative or complement to the charge-based conventional electronic technology, the nascent field "spintronics" has attracted much attention [1–5]. In quantum-confined nanostructures, the spin of electrons has shown an extraordinarily long spin dephasing time approaching microseconds [2–4] and a surprisingly large phase-coherent length of up to 100 μm [2]. These achievements provide intriguing clues for finding novel mechanisms not only for the functional improvement of conventional electronic devices, but also for information processing and transmission. Many potential applications of spintronics have been proposed, such as producing more efficient photoemitters with highly polarized electron beam, creating spin-memory devices [5] and spin transistors [6], and designing hardwares of spin quantum computers [7,8]. However, before any practical spintronic device can be demonstrated, more experimental progress as well as theoretical investigations are indispensable [9] to solve the fundamental questions, such as how to create and detect spin-polarized carriers and how to control their spin polarization and spin coherence for a relatively long time.

In semiconductor systems containing semimagnetic semiconductor(s) (SMS), due to the feasibility of engineering the band-offsets by an external magnetic field, a great deal of spin-related phenomena have been studied extensively in the past few years [10]. Recently, spin transport becomes one of the hot topics in these systems. Since the era of theoretical proposal by von Ortenberg [11] in 1982, spin superlattice was experimentally realized by Dai *et al.* [12], Chou *et al.* [13], and König *et al.* [14], respectively. Very recently, several groups have successfully injected spin-polarized current into a GaAs-based light-emitting diode with high efficiency. They used different Mn-based SMS as the spin-aligner. Fiederling *et al.* [3] used quaternary magnetic semiconductor (ZnBeMn)Se. Ohno *et al.* [4] chose Mn-doped GaAs. Jonker *et al.* [15] observed the maximal optical polarization (about 50%) using the ordinary paramagnetic ZnMnSe as the spin-injection contact. In these typical experiments, the systems work in the diffusive region. In the regime of ballistic spin-polarized transport, however, few experimental results have been reported. Theoretically, Egues studied the spin-dependent vertical transport through a $ZnSe/Zn_{1-x}Mn_xSe$ heterostructure in the ballistic region, where the structure has a single paramagnetic layer [16]. The results showed that one of the spin components of current density was strongly suppressed while the other varied slightly with the magnetic field increasing. So this system should behave as a good spin-filter. Further investigation on such a structure indicated the decreasing of polarization degree with the external electric field [17].

[a] e-mail: fzhai@castu.tsinghua.edu.cn

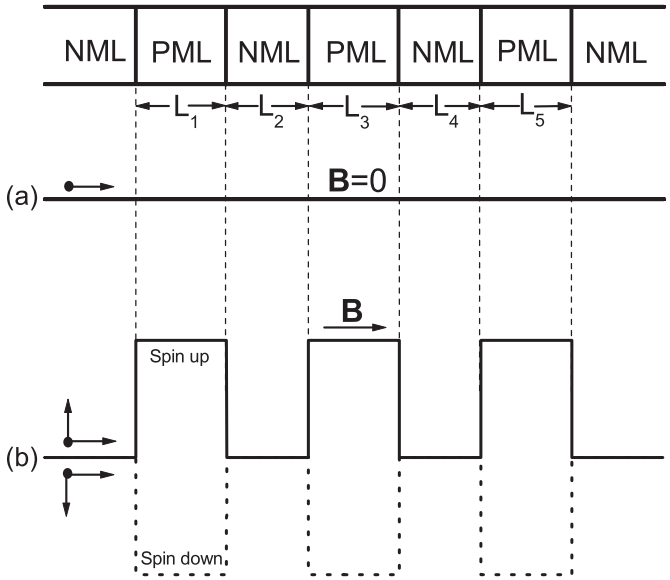

Fig. 1. A band-gap-matched ZnSe/$Zn_{1-x}Mn_xSe$ heterostructure with three paramagnetic layers and its conduction band profile. (a) Zero band-offsets in the absence of a magnetic field; (b) in an external magnetic field, the potential profile is spin-dependent: it is a double-well triple-barrier structure for spin-up electrons or a triple-well structure for spin-down ones.

In ZnSe/$Zn_{1-x}Mn_xSe$ heterostructures with double paramagnetic layers, Guo *et al.* examined spin-resonant suppression and enhancement [18] as well as quantum size effect and temperature effect [19].

In this work, we investigate the coupling effects of layers in the SMS heterostructure with triple paramagnetic layers, where the spin-dependent potential is a triple-barrier double-well structure for spin-up electrons and a triple-well structure for spin-down ones. It is well known that triple-barrier double-well electric structures possess more complex and interesting tunneling features than double-barrier structures, which is due to the presence of coupling between two quantum wells [20–23]. In addition, as mentioned above, the incorporation of local moments into semiconductor quantum structures brings a great diversity of phenomena. Therefore, one can expect a rich spin-dependent transmission behavior in the considered system. Our study indeed confirms this point. The results indicate that for electrons with either spin orientation transporting through an asymmetry structure, transmission resonances can be enhanced to optimum under both several positive and negative biases.

2 Model and formulation

The system we consider here is a band-gap-matched ZnSe/$Zn_{1-x}Mn_xSe$ heterostructure with three paramagnetic layers (PML) separated by double non-magnetic ZnSe layers (NML), which is depicted in Figure 1. L_1, L_3, L_5 are the widths of three PMLs, respectively; L_2, L_4 are the widths of two NMLs. In paramagnetic $Zn_{1-x}Mn_xSe$ layers, a homogeneous magnetic field B along the growth direction (taken as z axis) aligns the localized magnetic moments (originating from the half-filled $3d$-shell of Mn^{2+}) parallel to the field orientation, which provides an average spin $\langle S_z\rangle$ described by a modified 5/2 Brillouin function $\frac{5}{2}B_{5/2}(\frac{5}{2}g\mu_{\rm B}B/k_{\rm B}T_{\rm eff})$. Here $T_{\rm eff}(=T+T_0)$ is the effective temperature used to describe the Mn-Mn interaction phenomenologically [10]. The *sp-d* exchange coupling between the spin of conduction electrons and the localized magnetic moments gives rise to a spin-dependent potential V_{σ_z}. Within mean field approximation, V_{σ_z} is proportional to $\langle S_z\rangle$ and can be written as $V_{\sigma_z}=-N_0\alpha\sigma_z x_{\rm eff}\langle S_z\rangle$. Here, $N_0\alpha$ is the electronic *sp-d* exchange constant, σ_z represents the electron spin component ($\pm1/2$ or $\uparrow,\downarrow$), $x_{\rm eff}=x(1-x)^{12}$ is the effective Mn concentration used to account for the antiferromagnetic pair and x is the real Mn concentration. Note that V_{σ_z} is zero within the non-magnetic layers. Under an applied bias V_a along z axis, a term $-eV_az/L_t$ should be added to the effective potential, where L_t is the total length of the considered structure along the growth direction. The Hamiltonian of conduction electrons in this system can be written as

$$H=\frac{1}{2m^*}(\mathbf{P}+e\mathbf{A})^2-\frac{eV_az}{L_t}+V_{\sigma_z}, \tag{1}$$

where the electron effective mass m^* is assumed to be identical throughout the heterostructure, the vector potential is taken as $\mathbf{A}=(0,Bx,0)$.

The motion along z direction and that in the $x-y$ plane are separable when electrons are free of any kind of scattering. The quantized in-plane motion gives Landau levels with energy $E_n=(n+1/2)\hbar\omega_{\rm c}$, where $n=0,1,2,...$ and $\omega_{\rm c}=eB/m^*$. The electron motion along z axis can be described by a spin-dependent transmission coefficient $T_{\sigma_z}(E_z,B,V_{\rm a})$, which is determined from the reduced one-dimensional Schrödinger equation

$$-\frac{\hbar^2}{2m^*}\frac{{\rm d}^2\psi}{{\rm d}z^2}+U_{\sigma_z}(z)\psi=E_z\psi, \tag{2}$$

where E_z is the longitudinal energy of electrons and $U_{\sigma_z}(z)=V_{\sigma_z}-eV_az/L_t$ is the effective potential seen by a traverse electron, which includes effects of spin-dependent conduction-band discontinues at ZnSe/$Zn_{1-x}Mn_xSe$ boundaries as well as external electric and magnetic fields.

We determine the transmission using the scattering matrix method [24]. To begin with, we approximate the exact potential by a series of steps, which are thin enough so that over each step the potential can be treated as constant. As a result, the solution to equation (2) in the jth step is a superposition of plane waves:

$$\psi_{j,\sigma_z}(z)=A_{j,\sigma_z}{\rm e}^{{\rm i}k_{j,\sigma_z}(z-z_j)}+B_{j,\sigma_z}{\rm e}^{-{\rm i}k_{j,\sigma_z}(z-z_j)}, \tag{3}$$

where the wave vector $k_{j,\sigma_z}=[2m^*(E_z-U_{\sigma_z}(z_j))]^{1/2}/\hbar$ has non-negative imaginary part, z_j is the position of the

jth step's left-hand side, $j = 0, 1, 2, ..., N, N+1$ for a total of N steps. For simplicity, we assume all steps have the same width w, $z_0 = z_1 = 0$ and $z_{N+1} = L_t$. Imposing continuity of the wave function and its derivative at the boundary between step j and step $j+1$, one can relate the expansion coefficients $(A_{j,\sigma_z}, B_{j,\sigma_z})$ with $(A_{j+1,\sigma_z}, B_{j+1,\sigma_z})$ by a transfer matrix $\mathbf{M}_{\sigma_z}(j, j+1)$

$$\begin{pmatrix} A_{j,\sigma_z} \\ B_{j,\sigma_z} \end{pmatrix} = \mathbf{M}_{\sigma_z}(j, j+1) \begin{pmatrix} A_{j+1,\sigma_z} \\ B_{j+1,\sigma_z} \end{pmatrix}, \tag{4}$$

where

$$\mathbf{M}_{\sigma_z}(j, j+1) = \frac{1}{2} \begin{pmatrix} (1 + r_j^{\sigma_z})/s_j^{\sigma_z} & (1 - r_j^{\sigma_z})/s_j^{\sigma_z} \\ (1 - r_j^{\sigma_z}) s_j^{\sigma_z} & (1 + r_j^{\sigma_z}) s_j^{\sigma_z} \end{pmatrix}. \tag{5}$$

In this expression, $r_j^{\sigma_z} = \frac{k_{j+1,\sigma_z}}{k_{j,\sigma_z}}$, $s_j^{\sigma_z} = \mathrm{e}^{\mathrm{i}k_{j,\sigma_z} w}$ for $j > 0$ and $s_0^{\sigma_z} = 1$.

The scattering matrix $\mathbf{S}_{\sigma_z}(0, j)$ couples explicitly the outgoing states of the subsystem up to the jth step to the incoming states of the system as follows

$$\begin{pmatrix} A_{j,\sigma_z} \\ B_{0,\sigma_z} \end{pmatrix} = \mathbf{S}_{\sigma_z}(0, j) \begin{pmatrix} A_{0,\sigma_z} \\ B_{j,\sigma_z} \end{pmatrix}. \tag{6}$$

From the iterative relation [24] between $\mathbf{S}_{\sigma_z}(0, j+1)$ and $\mathbf{S}_{\sigma_z}(0, j)$ through the transfer matrix $\mathbf{M}_{\sigma_z}(j, j+1)$ and the fact that $\mathbf{S}_{\sigma_z}(0, 0) = \mathbf{1}$, we can evaluate the scattering matrix $\mathbf{S}_{\sigma_z}(0, N+1)$, which connects the transmission and reflection amplitudes with the incident amplitude.

By setting A_{0,σ_z}=1, B_{N+1,σ_z}=0, which corresponds to the situation that a spin electron is incident from the left-hand side of the system, the transmission amplitude A_{N+1,σ_z} is just $\mathbf{S}^{11}_{\sigma_z}(0, N+1)$, the (1,1) component of $\mathbf{S}_{\sigma_z}(0, N+1)$. The transmission coefficients, which are the ratio of transmitted particle flux to the incident particle flux, have the simple form as the following

$$T_{\sigma_z}(E_z, B, V_a) = \frac{k_{N+1,\sigma_z}}{k_{0,\sigma_z}} \left| \mathbf{S}^{11}_{\sigma_z}(0, N+1) \right|^2. \tag{7}$$

Note that the transmission coefficients depend on the traversing energy E_z, the magnetic field B, the applied bias V_a as well as the spin orientation.

We assume that the ZnSe layers are the emitter and collector attached to external leads. With E_f denoting the emitter Fermi energy, the Fermi-Dirac distribution function is $f(E) = \{1 + \exp[(E - E_f)/k_\mathrm{B}T]\}^{-1}$. The spin-dependent current density can be determined by [18]

$$J_{\sigma_z}(B, V_a) = J_0 B \sum_{n=0}^{\infty} \int_0^{+\infty} T_{\sigma_z}(E_z, B, V_a) \times [f(E_{n,k_z}) - f(E_{n,k_z} + eV_\mathrm{a})] \mathrm{d}E_z, \tag{8}$$

where $J_0 = e^2/4\pi^2\hbar^2$, $E_{n,k_z} = (n+1/2)\hbar\omega_\mathrm{c} + (\hbar^2 k_z^2/2m^*)$ are the energies of scattering-states.

3 Results and discussion

We consider the ballistic transport of a conduction electron traversing a band-gap-matched SMS heterostructure with three PMLs separated by two NMLs. To highlight the spin-dependent coupling between two NMLs, the widths of all PMLs are chosen to be equal ($L_1 = L_3 = L_5 = 20$ nm). Note that under an external magnetic field, each of paramagnetic layers act as a potential well for spin-down electrons and a potential barrier for spin-up ones. Thus the potential profile modulated by the external magnetic field is spin-dependent, which results in magnetic-field-tunable spin-polarization in this kind of structure [16–19]. In our considered system, spin-up electrons feel a triple-barrier double-well potential while spin-down ones see a triple-well counterpart, as shown in Figure 1. In addition, the asymmetry of the effective potential induced by the applied electric field makes the spin polarization also electric-field tunable [17–19].

Figure 2 presents the spin-dependent transmission coefficients for the case of two identical non-magnetic ZnSe layers ($L_2 = L_4 = 50$ nm). In all of the graphs, we use $m^* = 0.16\ m_\mathrm{e}$ (m_e is the free-electron mass), $x = 0.05$, $N_0\alpha = 0.26$ eV, $T = 4.2$ K, and $T_0 = 1.7$ K [14]. Under zero bias, the corresponding potential profile is symmetric triple wells for spin-down electrons or symmetric triple barriers for spin-up ones. Therefore, for electrons with both spin orientations tunneling through such a structure, unit quantum-resonances and resonance-splitting appear (see Figs. 2d1 and u1). As the traversing energy increases, the splitting space becomes larger and the dips between two adjacent splitting resonant peaks (SRP) go up. For the spin-up case, a wide forbidden region of transmission exists within two neighboring groups of splitting peaks, which is in contrast to the spin-down case. In the latter case, resonance is originated from the above-well virtual-states. As the bias increases, all transmission peaks shift towards low energy region and resonances are usually suppressed due to the electric-field-induced asymmetry. Under a small bias and for the spin-up case, the left one of the two splitting resonant peaks (LSRP) is lower and disappears earlier than the right counterpart (RSRP), which are clearly shown in Figures 2u2–u4. In addition, the dips between them drop off. As the applied bias increases, all LSRPs and dips are going down until to zero while the height of a RSRP varies non-monotonously. The reason is that the coupling between wells can (partly) compensate the bias-induced asymmetry. When the compensation is complete, the unit resonance appears, see Figure 2u4. As a result, one can see the transition between complete resonances and incomplete resonances [23] in the symmetric triple-barrier double-well structures. This is remarkable because in symmetric double-barrier structures, no electric-field-induced resonant enhancement occurs. In addition, when the LSRPs vanish, the doublet resonances turn to singlet resonances, which is similar to that depicted in reference [23]. At a higher bias, such as $V_\mathrm{a} = 5$ mV, the resonant splitting is not obvious and the resonance is suppressed in the considered energy region (Fig. 2u5). For spin-down case, however, the height of

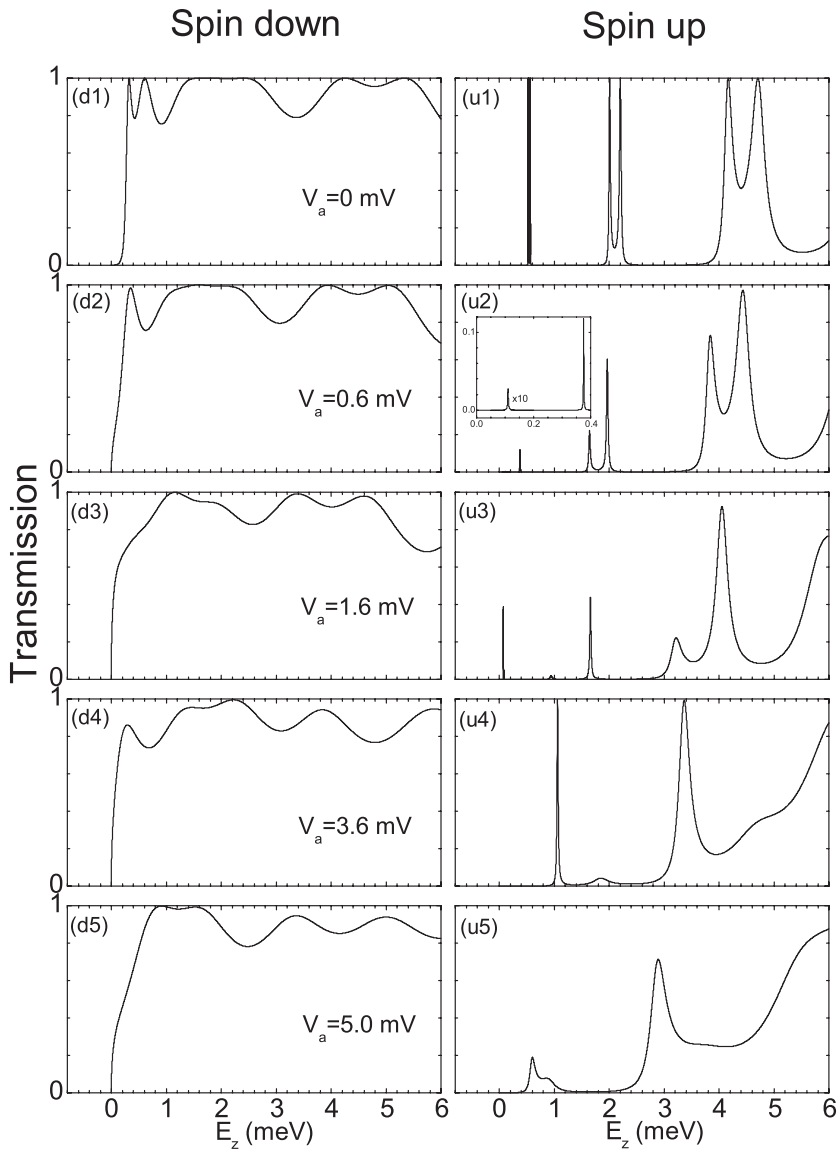

Fig. 2. Spin-dependent transmission coefficients for electrons traversing a symmetric ZnSe/$Zn_{1-x}Mn_xSe$ heterostructure with three paramagnetic layers under zero bias and several applied biases. All widths of paramagnetic layers are equal and set to be 20 nm. The two non-magnetic layers have the same widths $L_2 = L_4 = 50$ nm. $B = 2$ T. In the inset of panel (u2), the transmission is magnified with times 10 to show the first peak clearly.

transmission peaks varies slightly with the bias. Note that the transmission can also approach unit under a certain bias (Fig. 2d5), which is due to the presence of coupling among three wells.

Next we show the spin-dependent transmission coefficients for the case that double NMLs have different widths ($L_2 = 100$ nm and $L_4 = 50$ nm). At zero bias, it is obvious to see that resonances are suppressed (Figs. 3u1 and d1), especially for the spin-up case. This is originated from the structure-induced asymmetry. In addition, the resonant splitting is also clear and its features are similar to that of the symmetric structure under a small bias. For spin-up electrons tunneling through the asymmetric structure, it is easily seen that the transmission can be enhanced to optimal resonances under several positive biases (see Figs. 3u3 and u4). The electric-field-induced resonant suppression and enhancement in an asymmetric three-barrier electric structure was investigated by Allen and Richardson [20]. They introduced the asymmetry by adjusting barrier widths and heights. For spin electrons tunneling through an asymmetric SMS heterostructure with double PMLs, spin-dependent resonant suppression and enhancement were discussed in reference [18], where the structural asymmetry results from the difference of two PMLs. The studies indicated that some transmission peaks can be enhanced to unit under a certain positive bias for the spin-up case and under a certain negative bias for spin-down case. These optimal resonances are originated from the

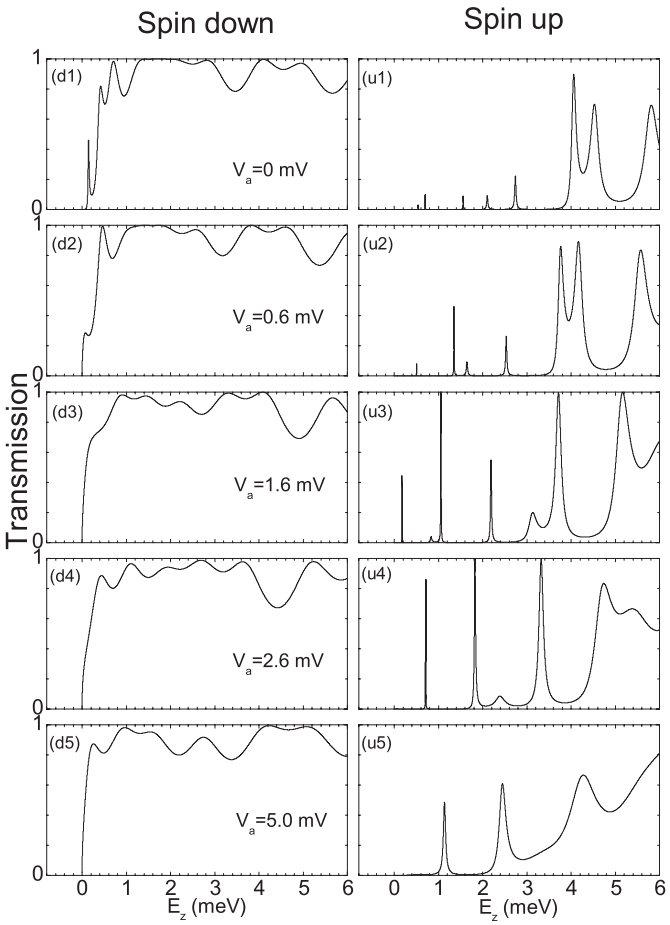

Fig. 3. Spin-dependent transmission coefficients for electrons traversing an asymmetric ZnSe/$Zn_{1-x}Mn_xSe$ heterostructure with three paramagnetic layers under zero bias and several positive applied biases. All widths of paramagnetic layers are equal and set to be 20 nm. The two non-magnetic layers have different widths $L_2 = 100$ nm, $L_4 = 50$ nm. $B = 2$ T.

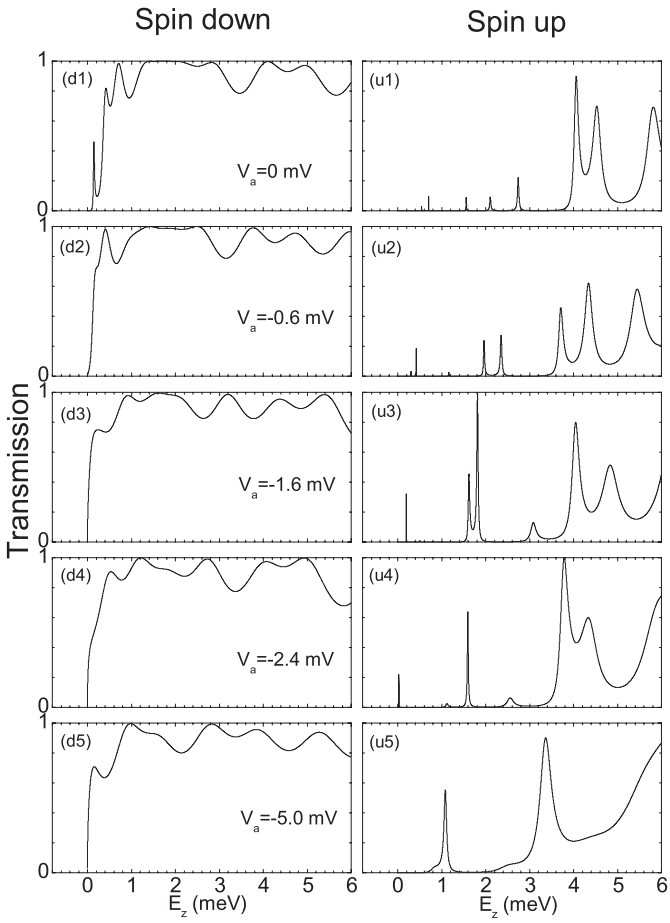

Fig. 4. Spin-dependent transmission coefficients for electrons traversing the same structure as that in Figure 3 under zero bias and several negative biases. $B = 2$ T.

complete compensation between the structural-induced as well as electric-field-induced asymmetry and the effect of bias on energies of quasi-bound states in the well (spin-up case) or on the coupling of above-well virtual-states in two quantum wells (spin-down case). In present work we introduce the structural asymmetry by adjusting only the widths of two NMLs. A very important result reported here is that under some negative biases, the resonant enhancement for the spin-up case can also occur in the structure considered here (see Figs. 4u3 and u4), which can not be seen in the double-barrier structure considered in reference [18]. Moreover, some peaks may approach unit under both a certain positive bias and a negative one with the same absolute value (see Figs. 3u3 and 4u3). The reason is that in three-barrier structure, the optimal resonance appears when the structure-induced and electric-field-induced asymmetry is completely compensated by the effect of bias on the coupling between the quasi-bound states in two quantum-wells. In such an asymmetric structure, on the other hand, a negative bias and a positive one modulate the interwell coupling with different ways, as they adjust the symmetry of the potential profile. Therefore, both of them at some special values may enhance the transmission. A remarkable and interesting phenomenon is that with the absolute value of bias increasing, the heights of most LSRPs decrease until to zero while those of most RSRPs first increase until to unit and then decrease. Accordingly, two types of transitions mentioned above occur. For spin-down electrons traversing the same structure, because of the presence of the coupling among three wells, the transmission can also be up to unit under a certain positive bias (see Fig. 3d2) or negative bias (see Fig. 4d4). Under a higher bias (for example, 5 mV), one could see the similarity of transmission behaviors between the symmetric and asymmetric structures.

In order to reveal the coupling effects of layers more clearly, Figure 5 plots the spin-dependent transmission in three kinds of (symmetric) SMS heterostructures labeled with "S", "D", and "T", which include single, double, and triple PML(s), respectively. The parameters are so chosen that all PMLs have the same width 20 nm and each NML within two adjacent PMLs has width 50 nm. At zero bias, for spin-down electrons transporting through the "S" structure, there is a peak in the transmission spectrum; while for spin-up ones traversing the same structure, the

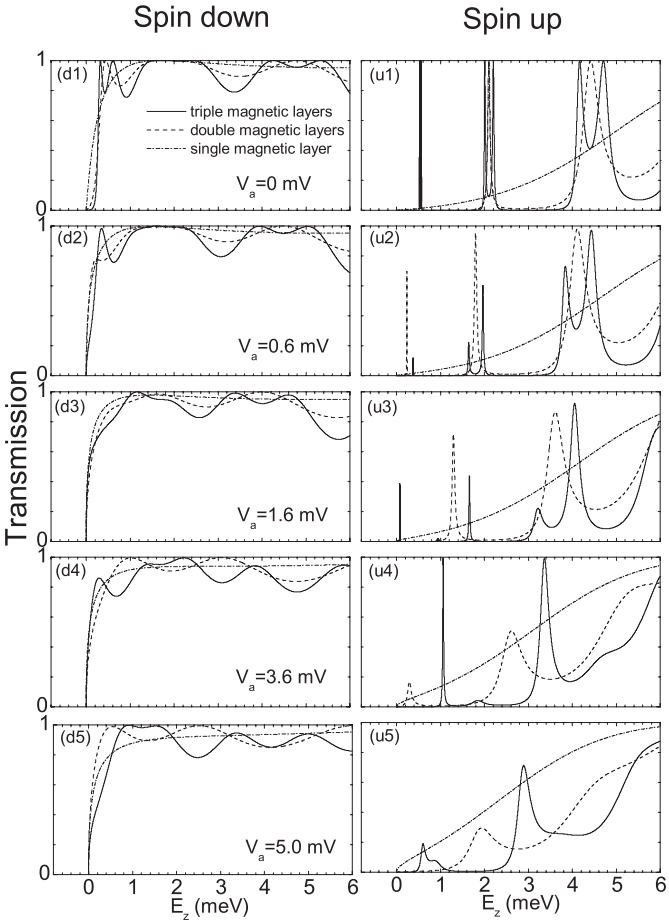

Fig. 5. Spin-dependent transmission coefficients for electrons traversing three different types of $ZnSe/Zn_{1-x}Mn_xSe$ heterostructures, which have single, double, triple semimagnetic layer(s), respectively. All widths of magnetic layers are equal and set to be 20 nm. All non-magnetic layers have width 50 nm. $B = 2$ T.

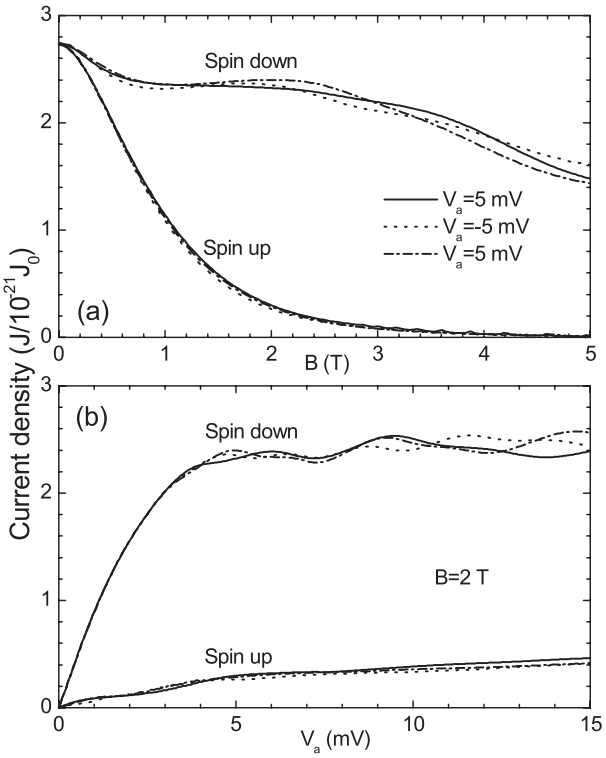

Fig. 6. Spin-dependent current densities for electrons traversing the $ZnSe/Zn_{1-x}Mn_xSe$ heterostructure with three paramagnetic layers. All widths of magnetic layers are equal and set to be 20 nm. $E_f = 5$ meV. Solid line: $L_2 = L_4 = 50$ nm; dash-dotted and dotted lines correspond to the heterostructure with $L_2 = 100$ nm, $L_4 = 50$ nm under positive and negative biases, respectively.

transmission is increasing monotonously with the longitudinal energy and no peak appears, which is due to the first virtual resonant state is beyond the considered region. For electrons with either spin orientation traversing the "D" or "T" structure at zero bias, one can see obvious quantum-resonances and some special E_z regions (called "excess region") where the transmission is not lower than that for the "S" structure. In addition, for the "D" structure, each resonant peak is just above the corresponding dip between a LSRP and RSRP; each "excess region" is covered by the corresponding counterpart of the "T" structure. It is notable that all dips locate on the transmission curve of the "S" structure. As the applied bias increases, all peaks shift to the low energy region while their heights vary distinctly in different structures. In the "S" structure, the transmission for spin-up electrons is moving up with the bias. For spin-down electrons, the transmission is decreasing with the bias when $E_z >$ 1.8 meV; the peak goes down until to disappear, thus the transmission is increasing monotonously with E_z (see the dash-dotted line in Fig. 5d5). In the "D" structure, the resonant peak for spin-up electrons drops with the bias while that for spin-down electrons varies slightly. In the "T" structure, however, because of the presence of coupling effects, the peaks show distinct variation with the bias. For spin-up electrons, a LSRP decreases up to zero; the height of a RSRP, however, oscillates with the bias: it first goes down then increases up to unit, and then decreases again (see the solid line in Figs. 5u1–u5). For spin-down electrons, one can also clearly observe the resonant suppression (see Figs. 5d4 and d5) and enhancement (see Fig. 5d5). For spin-down case, the "excess region" of the "D" structure and that of the "T" structure show complex variation with the bias. For spin-up case, this variation is clear. At small bias, the "excess region" of the "D" structure is not covered by that of the "T" structure (see Figs. 5u2–u4) because the dips (or LSRPs) are underneath the transmission curve of the "S" structure. Moreover, the total length of "excess region" of the "D" structure may exceed that of the "T" structure. At higher bias, such as $V_a = 5$ mV, the "excess region" of the "D" structure disappears while that of the "T" structure still exists. The reason is also due to the coupling effects between two wells.

Finally, we see to what extent the spin-dependent resonant enhancement and suppression are reflected in the magnitude of spin-dependent current density, which involves some kind of average of corresponding transmission coefficients. Figure 6a shows the current densities as the function of the magnetic field under a fixed bias with

absolute value $V_a = 5$ mV. At low magnetic field, the two components of current densities are nearly equal. As the magnetic field increases, the current densities split and the spin-polarization becomes more obvious due to the transmission suppression of spin-up electrons. One can see that under the same bias value, the spin-up current density ($J_\uparrow$) for the symmetric structure is slightly higher than that for the asymmetric structure. In addition, for the asymmetric structure under the negative bias, $J_\uparrow$ is slightly higher than that under a positive counterpart. it is notable that in certain magnetic field region, the spin-down current density ($J_\downarrow$) for the asymmetric structure under the positive bias is larger than that both for the symmetric structure and for the same structure under the reverse bias. The difference between $J_\downarrow$ for the asymmetric structure under negative bias and that for the symmetric structure fluctuates with the magnetic field. Figure 6b show the current densities as the function of the applied bias under a fixed external magnetic field $B = 2$ T. Note that the linear conductance (the ratio $J_{\sigma_z}(B, V_a)/V_a$ at the limit $V_a \to 0$) is obviously spin-dependent. As the applied bias increases, the discrepancy between $J_\uparrow$ and $J_\downarrow$ firstly increases with the bias then oscillates weakly. For spin electrons tunneling through an asymmetric heterostructure, the resonance enhancement and suppression can be clearly seen in both spin components of current density under both a positive bias and a negative one, which are originated from the enhancement and suppression in the transmission coefficients. Moreover, in the high-bias region (>4 mV), such effects for the spin-down case are more obvious than that for the spin-up case.

4 Conclusions

In this paper, we have investigated the coupling effects of non-magnetic layers or magnetic layers on spin-polarized transport through a SMS heterostructure with triple paramagnetic layers. The results indicate that for electrons with either spin orientation tunneling through either symmetric or asymmetric structures, obvious resonant enhancement can be seen in the transmission spectrum under several biases. Furthermore, for the asymmetric structure, optimal resonances may occur under both several positive and negative biases. The spin-dependent resonant enhancement is also clearly reflected in the spin-dependent current density. In addition, either in symmetric or in asymmetric heterostructure, the splitting transmission peaks show complicated variations with the bias, which is obviously displayed in the heights and locations of peaks. As the bias increases, most LSRPs decrease until to zero and vanish earlier than corresponding RSRPs, which usually increase until to unit then go down. Therefore, one can observe the transition from doublet resonances to single resonances and that between complete resonances and incomplete resonances. These interesting features are originated from the interplay between interwell coupling effects and effects induced by external electric and magnetic fields. We expect these interesting phenomena may shed some light on the development of spintronic devices.

This work was supported by the National Natural Science Foundation of China (Grant No. 10004006) and by the National Key Project of Basic Research Development Plan (Grant No. G2000067107).

References

1. G.A. Prinz, Phys. Today **48**, 58 (1995); Science **282**, 1660 (1998).
2. D.D. Awschalom, J.M. Kikkawa, Phys. Today **52**, 33 (1999).
3. R. Fiederling, M. Keim, G. Reuscher, W. Ossau, G. Schmidt, A. Waag, L.W. Molenkamp, Nature (London) **402**, 787 (1999).
4. Y. Ohno, D.K. Young, B. Beschoten, F. Matsukura, H. Ohno, D.D. Awschalom, Nature (London) **402**, 790 (1999).
5. J.M. Kikkawa, I.P. Smorchkova, N. Samarth, D.D. Awschalom, Science **277**, 1284 (1997).
6. D.J. Monsma, R. Vlutters, J.C. Lodder, Science **281**, 407 (1998).
7. D.P. DiVincenzo, Science **270,** 255 (1995); B.E. Kane, Nature (London) **393,** 133 (1998).
8. D. Loss, D.P. DiVincenzo, Phys. Rev. A **57**, 120 (1998); G. Burkard, H.A. Engel, D. Loss, Fortschr. Phys. **48**, 965 (2000).
9. S. Das Sarma, J. Fabian, X. Hu, I. Žutić, IEEE T. Magn. (1) **36**, 2821 (2000).
10. D.D. Awschalom, N. Samarth, J. Magn. Magn. Mater. **200**, 130 (1999).
11. M. von Ortenberg, Phys. Rev. Lett. **49**, 1041 (1982).
12. N. Dai, H. Luo, F.C. Zhang, N. Samarth, M. Dobrowolska, J.K. Furdyna, Phys. Rev. Lett. **67**, 3824 (1991).
13. W.C. Chou, A. Petrou, J. Warnock, B.T. Jonker, Phys. Rev. Lett. **67**, 3820 (1991).
14. B. König, U. Zehnder, D.R. Yakovlev, W. Ossau, T. Gerhard, M. Keim, A. Waag, G. Landwehr, Phys. Rev. B **60**, 2653 (1999).
15. B.T. Jonker, Y.D. Park, B.R. Bennett, H.D. Cheong, G. Kioseoglou, A. Petrou, Phys. Rev. B **62**, 8180 (2000).
16. J. Carlos Egues, Phys. Rev. Lett. **80**, 4578 (1998).
17. Y. Guo, H. Wang, B.-L. Gu, Y. Kawazoe, J. Appl. Phys. **88**, 6614 (2000).
18. Y. Guo, B.-L. Gu, H. Wang, Y. Kawazoe, Phys. Rev. B **63**, 214415 (2001).
19. Y. Guo, J.-Q. Lu, Z. Zeng, Q. Wang, B.-L. Gu, Y. Kawazoe, Phys. Lett. A **284**, 205 (2001).
20. S.S. Allen, S.L. Richardson, Phys. Rev. B **50**, 11 693 (1994).
21. L.D. Macks, S.A. Brown, R.G. Clark, R.P. Starrett, M.A. Reed, M.R. Deshpande, C.J.L. Fernando, W.R. Frensley, Phys. Rev. B **54**, 4857 (1996).
22. X.H. Wang, B.Y. Gu, G.Z. Yang, Phys. Rev. B **55**, 9340 (1997).
23. Y. Guo, B.-L. Gu, Z.-Q. Li, Q. Sun, Y. Kawazoe, Eur. Phys. J. B **3**, 257 (1998).
24. see, for example, D.Y.K. Ko, J.C. Inkson, Phys. Rev. B **38**, 9945 (1988); H.Q. Xu, Phys. Rev. B **50**, 8469 (1994).